

Synthesis of Hydroxyapatite-Ag Composite as Antimicrobial Agent

Dose-Response:
An International Journal
July-September 2020:1-14
© The Author(s) 2020
Article reuse guidelines:
sagepub.com/journals-permissions
DOI: 10.1177/1559325820951342
journals.sagepub.com/home/dos



Pamela Nair Silva-Holguín¹ and Simón Yobanny Reyes-López¹

Abstract

Innovative and improved antimicrobial agents by nanotechnology are developed to control and mitigation of resistant microorganisms. Nanoparticles of metals or oxide metals be able to be toxic to bacteria, demonstrating biocidal behaviors at low concentrations. The integration of silver nanoparticles in ceramic matrices has enhanced the antimicrobial performance, resulting in the search for new composites with improved bactericidal properties. The aim of this study was to prepare and characterize hydroxyapatite-silver nanocomposite and evaluate its antimicrobial properties against various Gram-positive and negative bacteria related to drug-resistance infections. Hydroxyapatite nanopowders were produced by sol-gel and silver nanoparticles were synthesized by reduction of Ag⁺ ions with the simple addition of gallic acid. Hydroxyapatite-silver composite (HAp-AgNPs) was prepared by adsorption of AgNPs at several concentrations. The results of UV-visible spectroscopy, dynamic light scattering, and transmission scanning electron microscopy revealed the existence of AgNPs with diameters around 6 nm. Scanning electron microscopy and energy dispersive X-ray spectroscopy corroborated the presence of silver disseminated over the surface of hydroxyapatite nanopowders. All HAp-AgNPs composites demonstrated excellent antibacterial effect even at lower silver concentration. HAp-AgNPs composites have a higher possibility for medical applications focused no the control of microorganisms with drug-resistance.

Keywords

nanocomposites, silver nanoparticles, hydroxyapatite, antibacterial activity, drug-resistance

Introduction

Drug-resistance infections for variety of virus, fungi and bacteria have increased extremely fast in the last years emerg like a grave health problem in the world. For this reason, it is important to develop new materials with higher antibacterial properties.¹ The high incidence of antibiotic-resistant bacteria coupled with the prevalence of dental caries and other diseases has led to the use of alternative antimicrobial agents. The overuse and misuse of antimicrobial agents as well as an absence of new antibacterial agents or materials have been the source of this antibiotic resistance crisis. For centuries, silver or silver compounds has been applied to avoid and care for a broad variety of infections, but its use has declined due to the discovery and innovation of a wide range of antibiotics. However, resistance caused by the abuse of various antibiotics has renewed the interest of the use of silver in infection control. The interactions that absorbed silver as with other metals and proteins in the human body do not be found to be dangerous and it has been revealed that silver is not toxic to humans.^{2,3}

The nanotechnology has provided a solid platform to produce an option for antibiotics to control bacterial infections. Nanomaterials offer elevated surface area to volume ratio with lower usage of materials leading to be more efficient in most applications, nanocomposites, and nanoparticles (NPs) are demonstrated antibacterial properties against to Gram-positive and Gram-negative bacteria.⁴ The search for novel biomaterials should also include antibacterial properties.

Hydroxyapatite (HAp) is commonly used in medical research as it has the comparable component of the mineral human

¹ Instituto de Ciencias Biomédicas, Universidad Autónoma de Ciudad Juárez, Envolve del PRONAF y Estocolmo s/n, Ciudad Juárez, Chih., México C.P.

Received 28 May 2020; received revised 19 July 2020; accepted 27 July 2020

Corresponding Author:

Simón Yobanny Reyes-López, Instituto de Ciencias Biomédicas, Universidad Autónoma de Ciudad Juárez, Envolve del PRONAF y Estocolmo s/n, Ciudad Juárez, Chih., México C.P. 32300.

Email: simon.reyes@uacj.mx



Creative Commons Non Commercial CC BY-NC: This article is distributed under the terms of the Creative Commons Attribution-NonCommercial 4.0 License (<https://creativecommons.org/licenses/by-nc/4.0/>) which permits non-commercial use, reproduction and distribution of the work without further permission provided the original work is attributed as specified on the SAGE and Open Access pages (<https://us.sagepub.com/en-us/nam/open-access-at-sage>).

skeleton. HAp has exceptional biocompatibility, great bioactivity, osteoconductive and chemical stability. To increase the mechanical property some polymers or ceramics are mixed to form HAp based composites. Hydroxyapatite shows low antibacterial property which leads to investigations focused on modifying doping bacteriostatic ions such as Sr, Zn, Ce and Ag.⁵⁻⁷ In general, the metallic nanoparticles generate more ions than in their presentation in micro or macro scale, therefore the quantity of ions and the bactericidal properties depend on their size.⁷⁻⁹

Silver nanoparticles (AgNPs) produce structural damage to the bacterial membrane and cell wall. The damage in DNA and RNA of bacteria inhibits bacterial reproduction.⁵⁻⁸ AgNPs have extraordinary well-recognized antibacterial properties. Silver nanoparticles were effective in killing a wide variety of bacterial pathogens involved in nosocomial infections such as *Staphylococcus aureus*, *Pseudomonas aeruginosa*, *Klebsiella pneumoniae*, *Klebsiella oxytoca* and *Escherichia coli*.¹⁻¹² The mechanism that has been reported is through the damage caused by Ag⁺ ions to the cell membranes of bacteria. The antibacterial efficacy of AgNPs is also known to depend on size, shape, dose, and time.⁶⁻¹² Triangular silver nanoparticles exhibit a better bactericidal effect than spherical and rod-shaped AgNPs, due to the high reactivity to silver in the basal plane (111), the reactivity of this plane has been reported for dendritic growth and formation of hot spots.¹² Ceramic–metal nanocomposites appear to expand the applications of biocide metals. Proteins, amino acids, and organic substances are easily adsorbed on the HAp surface, which in turn promotes the adsorption and replication of the bacteria on the HAp and consequently induces implant-related infections.⁶⁻⁸

The increasing interest in the use of AgNPs has been stimulated by the appearance and increment of drug-resistant bacteria. The new research proposes the use of silver nanostructures in a wide range of biomedical applications, exploiting their antibacterial properties.⁹ Ionic silver and AgNPs seem to reveal a similar mechanism of action on the target membrane, although AgNPs are more efficient at lower concentrations than ionic silver.¹⁰ Therefore, silver containing in HAp composite fusing biocompatibility, great bioactivity, osteoconductive and chemical stability of HAp with the antibacterial effect of Ag to give a great potential application in bone substitute materials or in coating metal implants to prevent implant-related infections.¹¹⁻¹⁸

There are several methodologies available for the synthesis of silver nanoparticles: reduction in aqueous systems, chemical reactions, photochemical, thermal decomposition of silver compounds, radiation, electrochemical, sonochemical, microwave chemical routes and recently green methodologies.⁹⁻¹⁹ Green synthesis methodologies of synthesis of silver nanoparticles have proven to be better practices, allow manipulation, control overgrowth and stabilization, allowing application in nanomedicine, avoiding the use of toxic products in the synthesis protocol. Gallic acid (GA) has been used as a green reducing agent to synthesize Au and Ag nanoparticles. Gallic acid synthesis is considered green because it is done in a single step without adding any stabilizing agent or chemical substances. GA is found in a variety of plants, such as spinach, grapes, green tea and oak bark, as well as in their products (red wine or white

wine). The GA has been attributed properties as an antioxidant, antibacterial, antiviral, anti-inflammatory and anticancer.¹⁷ AgNPs turn out to be toxic to human cells in concentrations greater than 1% and in prolonged treatments causing argyria. Therefore, it is necessary to develop materials at low concentrations to obtain a bactericidal effect without cytotoxic impact.¹⁻²⁵ Administration of AgNPs as a bactericidal treatment requires a vehicle; HAp could satisfy this purpose.⁵⁻¹¹

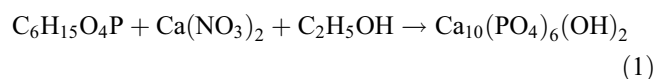
Silver nanoparticles have been used in a wide variety of biodegradable materials to give them an antibacterial character. The studies mention for example: the synthesis of hydrogels of biodegradable nanocomposites using green chemistry processes, utilized acrylamide with I-Carrageenan and reduce silver with *Azadirachta* leaf extracts for the inhibition of *Bacillus* and *E. coli*, with applications in medical devices,²⁴ deposition of silver nanoparticles on biodegradable phosphate ceramic surfaces with an antibacterial effect against *E. coli*, where the antibacterial effect could occur when the microorganism adsorbs the minerals from the material and releases the nanoparticles into the medium,²⁵ lignin biopolymer nanoparticles with silver ions as nuclei coated with a layer of a cationic polyelectrolyte to help the nanoparticles bond with the bacterial membrane producing a biocidal action on *E. coli* and *P. aeruginosa*,²⁶ films of PVA, nanocellulose and silver nanoparticles with great antibacterial activity also been prepared against *S. aureus* (MRSA) and *E. coli*.²⁷

Biocompatibility and antibacterial properties are the most important factors in designing novel biomaterials. The biocompatibility of HAp and the antibacterial power of AgNPs will allow to form a composite material to release NPs and Ag⁺ ions. The principal aim of this contribution is to develop an inexpensive, effective, and aqueous procedure for synthesis of HAp-AgNPs composite and evaluate their antibacterial performance on Gram-positive and negative bacteria related to drug-resistance infections at low concentration of silver to resolve to control microorganisms of clinical importance.

Materials and Methods

Synthesis of Hydroxyapatite

Calcium nitrate tetrahydrate (Ca(NO₃)₂·4H₂O, CaN), triethyl phosphite ((C₂H₅O)₃P, P(OEt)₃) and ethanol were used as raw materials to synthesize the sol, all chemicals were obtained from Sigma-Aldrich Co. This synthesis was carried out employing the method reported previously by Garibay in 2017.²² The Ca(NO₃)₂ was dissolved and the P(OEt)₃ was hydrolyzed in ethanol. The CaN solution was added by dripping to the triethyl phosphite during under stirring for 24 h at 40°C, after time the temperature was increased to 60°C for 24 h under constant stirring to form a viscous white liquid. The resulting gel was dry and heat treated to obtain a solid mass at 970°C for 3 h according to reaction (1). To obtain the powdered gel of HAp was crashed in agate mortar.



Synthesis of AgNPs

The synthesis of silver nanoparticles was from chemical reduction, in which silver nitrate was used as a metal precursor, gallic acid as a reducing agent and sodium hydroxide as a stabilizing agent. A 10 mM silver nitrate solution was made, to which the reducing agent was added and immediately afterward, sodium hydroxide (1 M) was added dropwise to a pH of 11.

Synthesis of HAp-AgNPs

The composite of HAp-AgNPs was carried out through simple adsorption by mixing the hydroxyapatite powders with the solution of silver nanoparticles under constant stirring at room temperature for 72 h, after the time passed, the solution was filtered under vacuum and dried at 100°C for 24 h and after 200°C for 3 h. Four concentrations of HA-AgNPs powders (0.5, 1, 2.5 and 5 mM) were prepared.

Characterization

UV-Vis spectra were evaluated at 25°C in a Cary100 spectrophotometer (Varian Corp.) using a 10 mm quartz cell. Particle size and distribution were calculated by dynamic light scattering (DLS) in a Nanoparticle Analyzer SZ-100 (HORIBA). Field Emission Scanning Electron microscope SU5000 Hitachi was used. Vibrational bands of bonds and functional groups present in samples were determined by Fourier Transformed Infrared Spectroscopy (FTIR), using a Bruker Alpha Platinum ATR spectrometer and Raman spectrophotometer alpha300 R, with a 532 nm laser. X-Ray Diffraction was employed to identify crystalline phases present in the samples in instrument X'Pert PRO PANalytical, with $\text{Cu } k\alpha = 1.54$, 20 kV, in the range of 2θ of 10 to 80°, a 2°/min scanning speed by the powder method. Thermal evolution of sample was determined by Thermogravimetric Analysis and Differential Scanning Calorimetry, using an SDT Q600 V20.9 Build 20 instrument.

Antibacterial Activity

Disk diffusion method was performed to measure antibacterial activity of HAp-AgNPs composites against *E. coli*, *K. oxytoca*, *P. aeruginosa*, *S. mutans*, *S. aureus*, and *B. subtilis*. The microbial species were cultured in Müller-Hinton broth for 20 h at 37°C before the test. According to the McFarland scale (1.3×10^6 CFU/mL), 100 μL of standardized suspensions of each bacterium was placed on Müller-Hinton agar plates. 0.05 g of the synthesized composites was weighed before they were used for the antimicrobial activity study. The agar plate was divided into 5 sections to adapt each of the samples. Antibacterial tests were carried out by adapted the disc diffusion method using the suspension of bacteria spread on a Mueller-Hinton agar plate. The inoculated plates were incubated for 24 h at 37°C. The antibacterial effect was determined by the measurement of clear zones resultant to inhibition formed around the composites with a caliper. All tests for each microorganism were made in triplicate.

Minimum Inhibitory Concentration (MIC) was determined using the microbroth dilution method in a microplate reader Multiskan MCC Fisher Scientific. The procedure for the evaluation of the antimicrobial effect of the different samples was based on the same Gram-positive and Gram-negative bacterial culture. For the turbidimetry method, the test was carried out in a 96-well microplate where 200 μL of the standardized inoculum of each bacterium and 5 mg of each treatments were placed, the microplate was incubated at 27°C for 24 h with constant agitation, after the time the optical density was determined and by percentage calculations the percentage of inhibition was determined. Measurements were carried out at time 0, then each half-hour for 24 h at 37°C, at a wavelength of 570 nm. The antimicrobial test for all microorganisms and composites was made in triplicate. After that time, the final absorbance was measured to estimate the inhibition percentage. All data were analyzed by IBM SPSS Statistics 25 and are expressed as mean values \pm SE. Statistical analyses were carried out using ANOVA and Tukey's multiple comparison test. A p value ≤ 0.05 was considered statistically significant.^{4,20}

Results and Discussion

Synthesis of Hydroxyapatite

The thermogram of the synthesized HAp shows 3 different stages of decomposition. The first stage occurs between 35 to 120°C due to the loss of ethanol and water, the second from 120 to 290°C where the decomposition of ammonia and dehydration occurs, the third stage occurs between 290 and 480°C by decomposition of nitrate and structural water according previous results.²² The UV-vis spectrum shown in Figure 1A shows a marked absorbance at 300 nm, absorbance recorded on the ultraviolet region of the electromagnetic spectrum corresponding to the hydroxyapatite. The infrared spectrum of Figure 1B shows bands at 560, 600 and 628 cm^{-1} corresponding to flexural vibrations of the phosphate group (PO_4^{-3}),^{13,14,22} and bands at 961, 1022 and 1090 cm^{-1} corresponding to symmetric phosphate group vibrations.^{13,14} The Raman spectrum of the HAp presented bands at 435, 590, 964, 1049 and 1081 cm^{-1} , the band at 964 cm^{-1} being the most intense as seen in Figure 1C, the bands located at 435 and 590 cm^{-1} can be attributed to the flexural modes of the phosphate group, the 964 cm^{-1} band is a typical phosphate band associated with carbonated apatite, while the 1049 and 1081 cm^{-1} bands are associated with the vibration modes of stretching of the phosphate group.¹⁴ According to Raman and infrared spectroscopy analysis, the presence of phosphate groups in the synthesized hydroxyapatite is confirmed, without the presence of bands corresponding to precursors used. EDX analysis shows the elemental composition of the HAp, where intensities associated with calcium, phosphorus and oxygen were identified (Figure 1D). The results are consistent with the chemical composition of the HAp of OH^- , Ca^{+2} and PO_4^{-2} .¹⁵ The elementary percentage of the synthesized HAp is: 45% calcium, 38% phosphorus and 16% oxygen. The Ca/P ratio obtained was ~ 1.53 , compared to the ideal 1.67

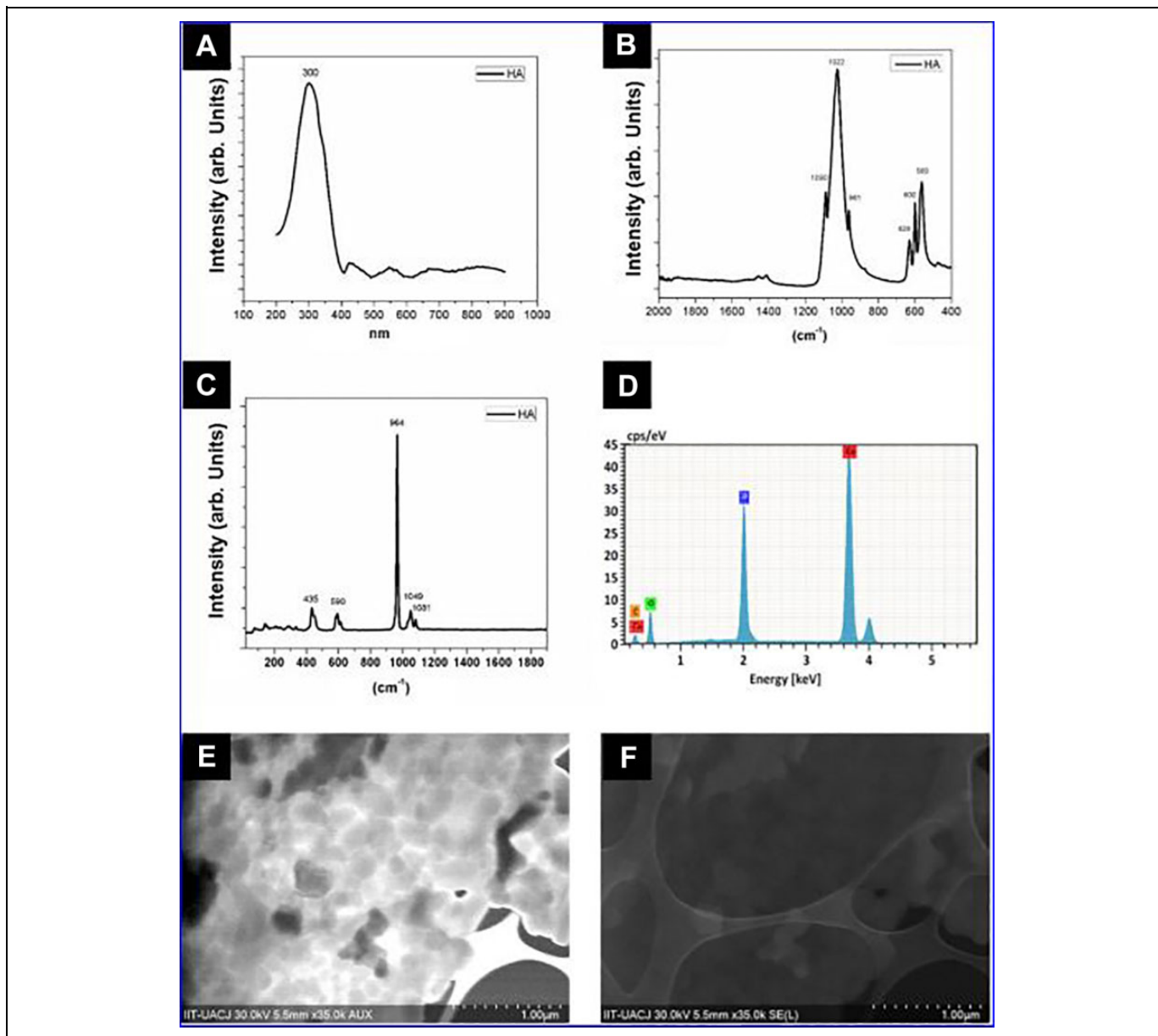


Figure I. Synthesized hydroxyapatite, UV-Vis spectrum (A), infrared spectrum (B), Raman spectrum (C), EDX analysis (D), STEM micrographs backscattered (E) and secondary electrons (F).

ratio of HAp.¹⁶ The elementary distribution by EDS confirmed that calcium and phosphorus are distributed homogeneously. STEM images revealed a morphology in semi-hexagonal agglomerated plates with each other as seen in Figure 1E and F. By dynamic light scattering (DLS) a particle size of 263 ± 23 nm was obtained for the synthesized HAp, particle size confirmed by measuring the particles by scanning electron microscopy, obtaining a size of 220 ± 63 nm. A zeta potential of -37.4 ± 2.5 mV of the hydroxyapatite was determined, indicating that it is moderately stable.

Synthesis of silver nanoparticles. The silver nanoparticles were synthesized by the chemical reduction method, in which a

slightly viscous reddish-brown solution was obtained that when diluted turned yellow. Figure 2A shows the transmission electron microscopy micrograph of silver nanoparticles with spherical, non-agglomerated morphology and diameters between 5 to 10 nm. The UV-vis spectrum Figure 2B showed a pronounced absorbance at 410 nm which corresponds to the Surface Plasmon Resonance (SPR) of the silver nanoparticles with sizes from 5 to 20 nm,¹⁷ supporting the DLS results. A band at 290 nm is also observed in the UV-vis spectrum due to the presence of the reducing agent (gallic acid). According to TEM images and UV-vis spectrum, AgNPs are spherical and without agglomerations, showing the stabilizing effect of gallic acid. Particle size determined by dynamic light scattering presented

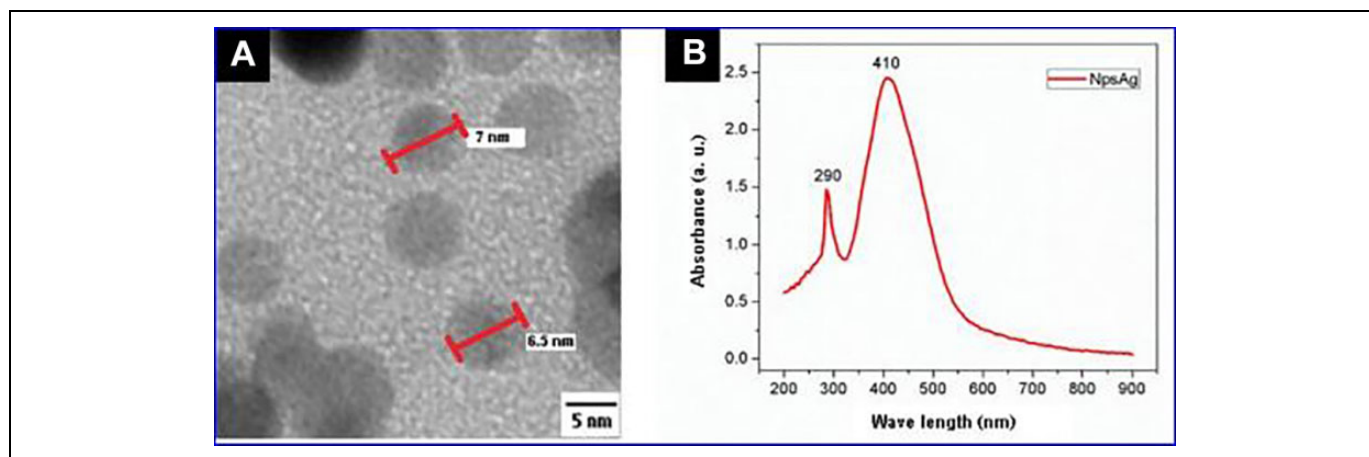


Figure 2. Transmission electron microscope micrograph of AgNPs (A) and their UV-vis spectra (B).

a size of 5.6 ± 2.9 nm and zeta potential of -55 ± 3.4 mV, indicating that they have good stability.

Synthesis of HAp-AgNps. HAp powders were obtained with AgNPs at concentrations of 0.5, 1, 2.5 and 5 mM shows an intensification in brown tonality as the concentration of silver increases (Figure 3F), from a white of the HAp, to an ochre brown with 0.5 mM, a brown brown in 1 mM, a brown in 2.5 mM and a dark coffee at 5 mM. The actual concentration of silver nanoparticles in the powders was determined by measuring the residual liquid and a calibration curve, thus obtaining a real concentration of 0.497, 0.975, 2.495 and 4.993 mM for the theoretical concentrations of 0.5, 1, 2.5 and 5 mM respectively.

In the UV-vis spectrum of the HAp-AgNPs powders of Figure 3A a marked absorbance at 290 nm corresponding to HAp is observed, while for the higher concentrations of AgNPs (2.5 and 5 mM) an absorbance at 422 nm is presented (Figure 3B), this band can be caused by the resonance of the surface plasmon of the AgNPs. In an article published by Hye-hyun, in 2018, an AgNPs SPR displacement of 410 nm at 443 nm was observed with the presence of HA, because the metal nanoparticles were impregnated on the surface of HA. A shift toward longer wavelengths of the SPR is associated with its increase in particle size.¹⁷ The infrared spectra of Figure 3C for HAp-AgNPs composites at concentrations of 0.5, 1, 2.5 and 5 mM shows 3 bands in 563, 599, 637 cm^{-1} which are attributed to the flexural vibration of the phosphate (PO_4^{3-}) functional group of HA and other more intense bands at 960, 1028 and 1090 cm^{-1} corresponded to a symmetric phosphate group vibration in addition to a very weak band at 875 cm^{-1} due to the vibration corresponding to a CO_3^{2-} group. For the spectra of HAp-AgNPs at all concentrations the same bands as in HA are observed, indicating that there is no structural change. The Raman spectrum in Figure 3D for HAp-AgNps powders at the concentrations of 0.5, 1, 2.5 and 5 mM presents the HAp bands in addition to a broadening of the spectrum of the initial part corresponding to the fluorescence. The bands at 429 and 450 cm^{-1} can be attributed to the O-P-O bending modes, the

frequencies for PO_4^{3-} are associated at 589 and 606 cm^{-1} , for the O-P-O bending character. The band at 961 cm^{-1} is a typical phosphate band associated to the carbonated apatite. Finally, the bands at 1045 and 1075 cm^{-1} are assigned to the P-O stretching vibrational modes.¹⁴ In these spectra it can also be observed that the intensity of the HAp peaks increases at the lowest concentration of AgNPs (0.5 mM) related to the presence of low concentration of silver, this can be attributed to the contribution generated by the dopant AgNPs. It has been reported that noble metals at low concentration can be display a scattering enhanced in Raman spectroscopy.¹⁴ The intensity of bands decreases as the concentration of silver used increases associated to the concentration of silver and agglomeration and loss the crystallinity of HAp particles in the aqueous media. Figure 3E shows an X-ray diffraction pattern of HAp and HAp-Ag nanocomposites all the peaks observed can be associated to the structure of the HAp according to the reported JCPDS no. 00-009-0432.¹⁴ HAp exhibits a great affinity with the AgNPs which the results suggest that the adsorption process of the AgNPs was carried out onto the HAp surface, but in this case a peak of silver are present at low intensity.

Figure 4 shows the SEM micrographs of 0.5, 1, 2.5 and 5 mM HAp-AgNPs powders, where the effective presence of AgNPs in HAp can be observed, the contrast of AgNPs is clearly shown (in spherical form) adhered to the surface of the HAp. For the concentration of 0.5 mM, a particle size of 22.03 ± 13.79 nm and a zeta potential of -31.7 ± 1 mV were obtained indicating a moderate stability whereby there is agglomeration between the particles as seen in Figure 4A and B. At a concentration of 1 mM a particle size of 18.49 ± 4 nm and a zeta potential of -44.2 ± 1.6 mV were obtained, and the particles have smaller size and slight agglomeration as shown in Figure 4D and E. For 2.5 mM, there is a greater abundance of particles, grouped without agglomerating with a particle size of 10.53 ± 1.56 nm and zeta potential of -46.6 ± 1.2 mV (Figure 4G and H). In the case of the 5 mM concentration, there is an abundance of particles distributed throughout the sample with sizes of 9.76 ± 2.59 nm and zeta potential of -45.2

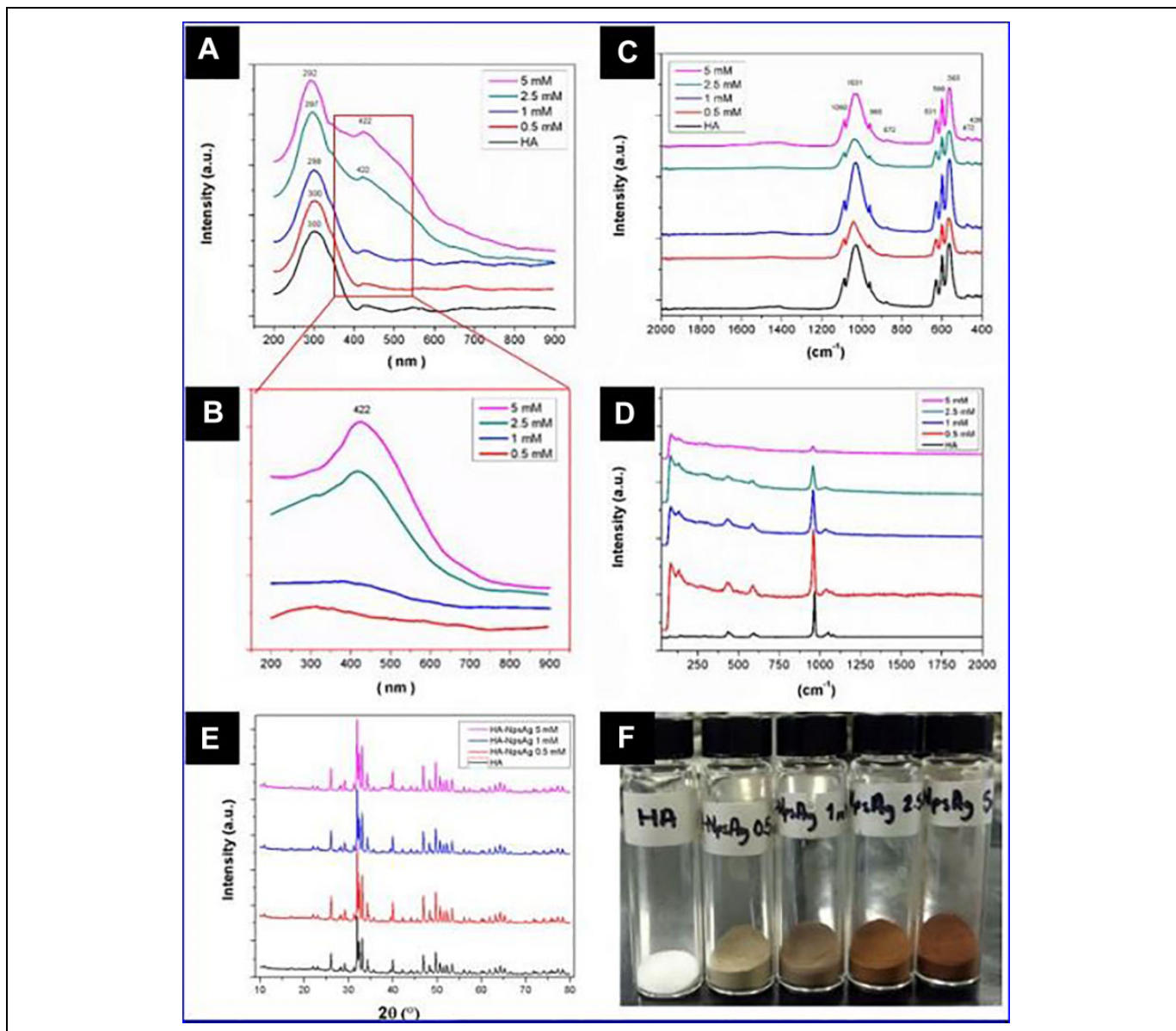


Figure 3. UV-vis spectrum (A), UV-vis spectrum magnification (B), FT-IR spectrum (C), Raman spectrum (D), X-ray diffractogram (E), HAp-AgNPs image, from left to right, HAp, HAp- AgNPs at 0.5, 1, 2.5 and 5 mM (F).

± 1.5 mV, smaller particles are observed here without agglomeration (Figure 4J and K). The micrographs of HAp-AgNPs powders by SEM gives the presence of spherical silver nanoparticles on the entire surface of the hydroxyapatite and by increasing the concentration of AgNPs more surface of the HAp is cover. The EDX analyzes of 0.5, 1, 2.5 and 5 mM powders respectively are shown in Figure 4C, F, I and L. Intensities associated with the presence of calcium, phosphorus, oxygen and carbon due to HAp were identified. In addition to that, the intensity associated with silver also increases as the concentration of AgNPs in HAp powders increases (from top to bottom). For the concentrations of 0.5, 1, 2.5 and 5 mM, 0.32, 0.42, 2.13 and 5.67% of silver were obtained, respectively.

Figure 5 shows the elemental distribution maps of 5 mM HAp-AgNPs powder by EDX. In 5-A the SEM micrograph by secondary electrons is observed, the distribution of silver throughout the sample and small agglomerates resulted in brightest points, in 5-B the silver in red color shows how it is distributed throughout the surface of the hydroxyapatite, and the intensity increase where more silver is deposited, 5-C the distribution of calcium in green corresponds to the entire area of hydroxyapatite analyzed, in 5-D the distribution of phosphorus follows the same distribution of calcium, in 5-E the distribution of the oxygen follows the pattern of hydroxyapatite particles and finally in 5-F the carbon distribution corresponds to the hydroxyapatite also analyzed in the micrograph.

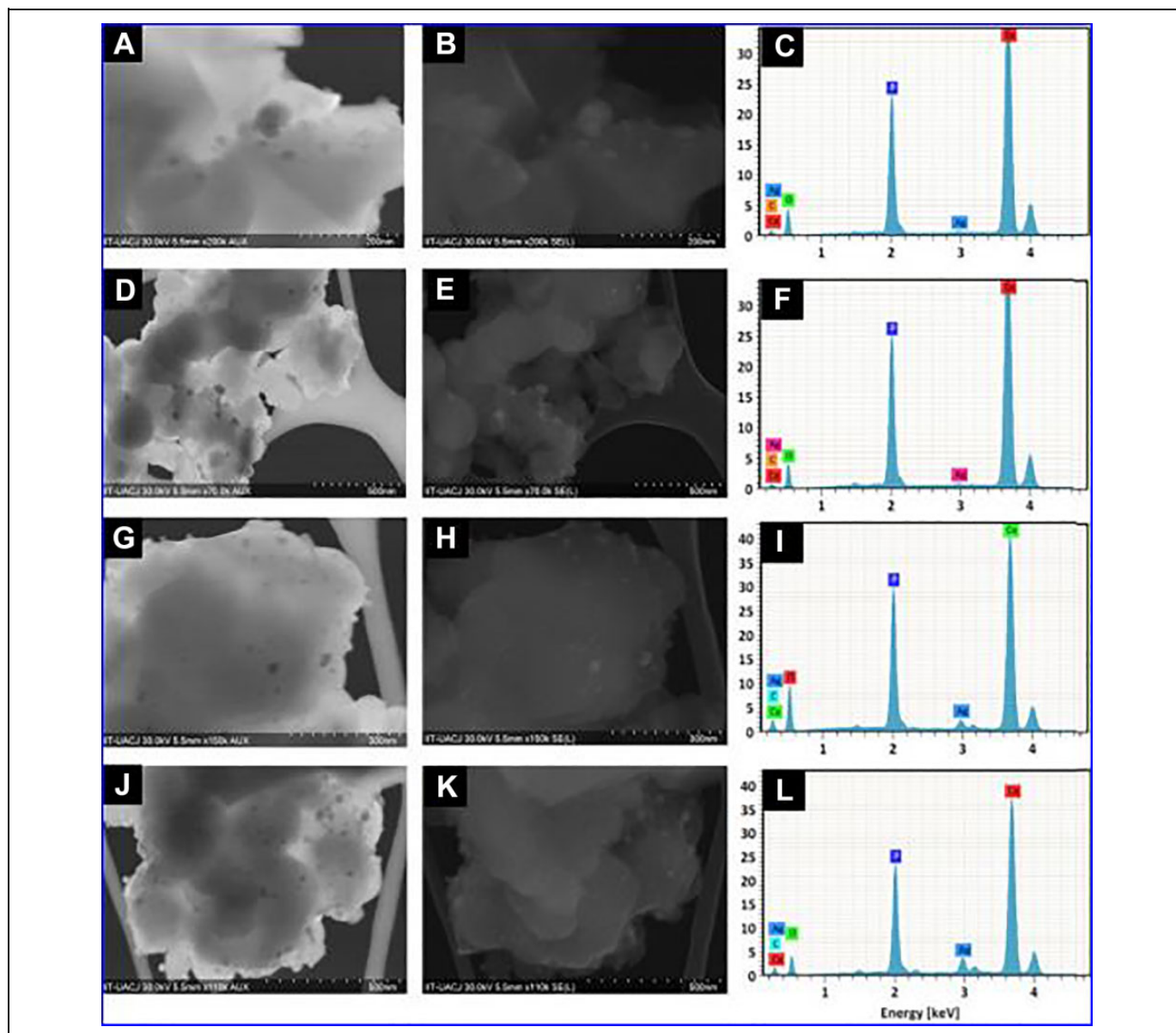


Figure 4. STEM micrographs of HAp-AgNPs powder at: 0.5 mM (A), 1 mM (D), 2.5 mM (G) and 5 mM (J). MEB-SE micrographs of HA- AgNPs powder at: 0.5 mM (B), 1 mM (E), 2.5 mM (H) and 5 mM (K). EDX analysis of 0.5 mM (C), 1 mM (F), 2.5 mM (I) and 5 mM (L).

The mechanism of metal adsorption onto hydroxyapatite is ionic exchange. This process consists in 2 subsequent steps. First, negative charges formed on the surface of hydroxyapatite dissociates into Ca^{+2} and H_2PO_4^- , in the second step, Ca^{+2} ions located in the surface are exchanged with silver nanoparticles present in the medium. Another second mechanism is by the interaction of silver hydrated nanoparticles by diffusion into the porous structure of HAp powders. Furthermore, the formation of a new phase in the adsorption process is discarded due to the absence of other peaks in the XRD analysis. With the data obtained in Figure 6, the tendency can be observed that, by increasing the concentration of silver, the zeta potential increases and the particle size decreases, avoiding the formation of agglomerates, thus demonstrating the good distribution

of silver on the HAp particles, producing a compound with good electrostatic stability.

Antibacterial activity. Figure 7 shows the photographs of the powder inhibition halos for all the bacteria used. The disk diffusion method demonstrated the sensitivity of bacteria to HAp-AgNPs powders at different concentrations of silver nanoparticles. The inhibition halos when compared show that the higher the concentration of silver nanoparticles, the greater the inhibition halo. It is also shown that the bacteria most susceptible to AgNPs is *Pseudomonas aeruginosa* and the least susceptible is *Bacillus subtilis*. The results indicate that all the bacteria used were susceptible to HA- AgNPs powders, with *Pseudomonas aeruginosa*, *Escherichia coli* and *Klebsiella oxytoca* being the most

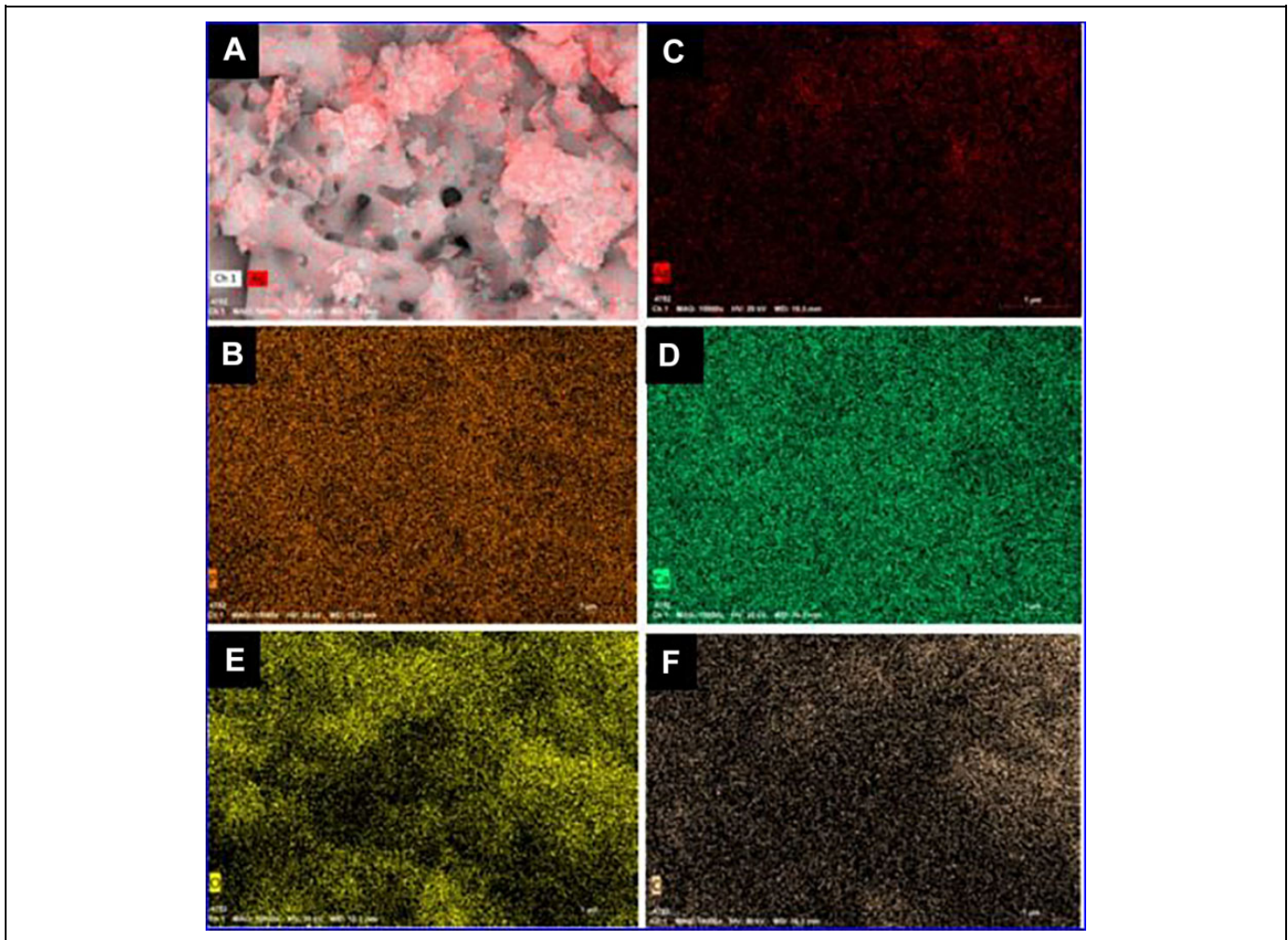


Figure 5. Compositional analysis EDX_SEM of 5 mM HAP-AgNPs: A) micrograph on secondary electrons, B) silver, C) phosphorus, D), calcium, E) oxygen and F) carbon.

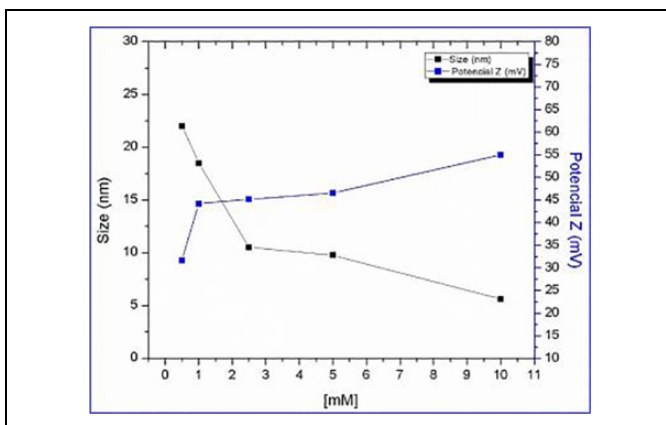


Figure 6. Particle size versus zeta potential.

susceptible and the least susceptible *Bacillus subtilis*, *Staphylococcus aureus* and *Streptococcus mutans*.

Figure 8 illustrate a Tukey analysis with a significance level of 0.05 and using the inhibition halos as a response variable, it

was observed that from the concentration of 0.5 mM a significant effect on the inhibition was obtained of the bacteria used. Figure 8 shows that *E. coli* and *S. mutans* do not show a significant difference in inhibition halos for the 4 concentrations used and indicates that *E. coli* and *S. mutans* are not as sensitive to variation of the concentration of the AgNPs. In the case of *P. aeruginosa* and *B. subtilis* the concentrations of 0.5 and 1 mM and 2.5 and 5 mM do not have a significant difference between them respectively, the above indicates that *P. aeruginosa* and *B. subtilis* are not sensitive to changes in concentration double the AgNPs. Finally, *K. oxytoca* and *S. aureus* have a significant difference between the 4 concentrations, which means that they are sensitive to the variations of the AgNPs.

Antimicrobial effect by turbidimetry. The antibacterial effect was also determined by the turbidimetry method and the percentage of inhibition of each concentration of silver nanoparticles with each bacterium was obtained. Figure 9 shows that the bacterium that most inhibited HAP-AgNPs dust by this method was *Pseudomonas aeruginosa* with a percentage of inhibition of

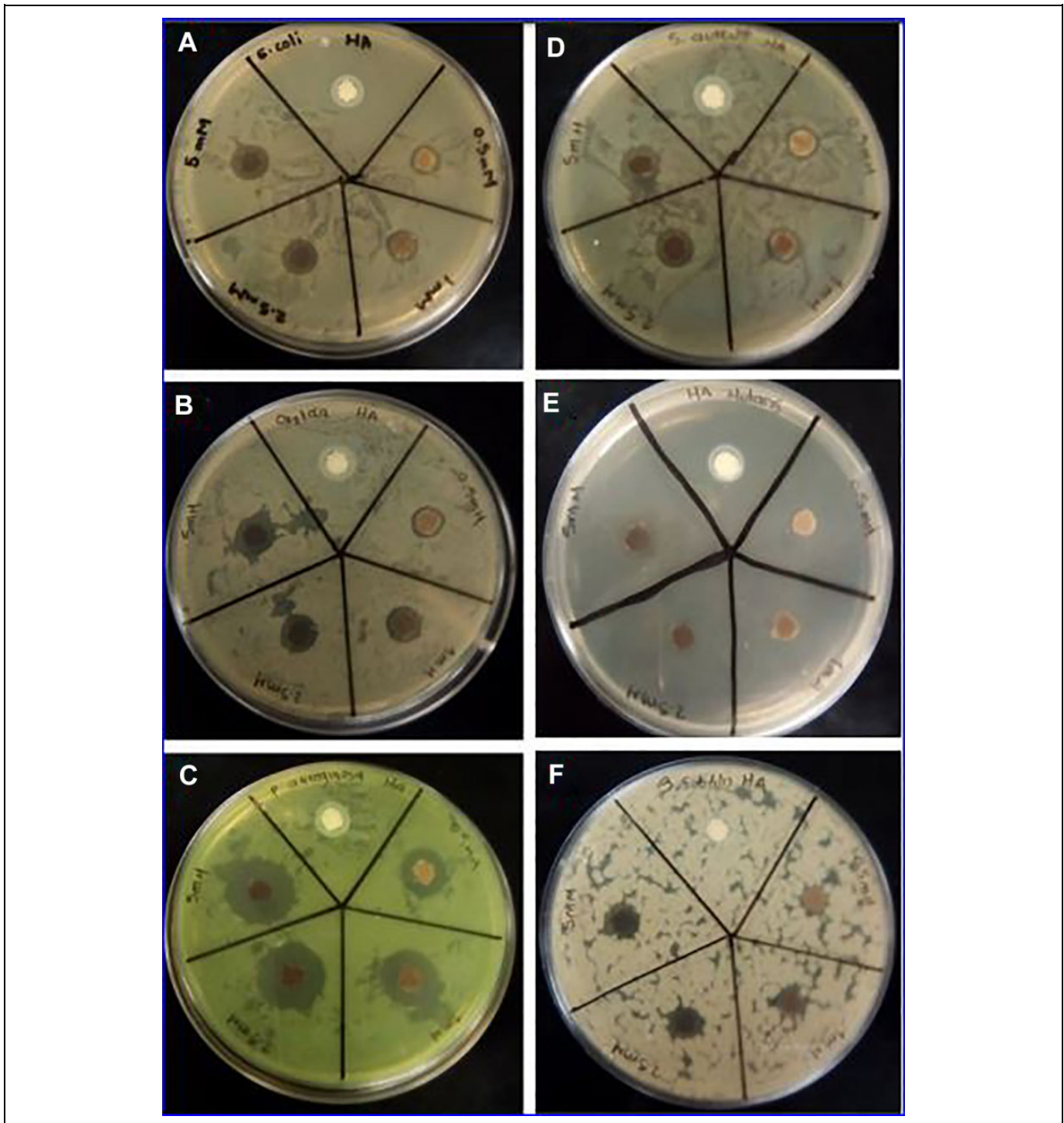


Figure 7. Inhibition halos for: A) *Escherichia coli*, B) *Klebsiella oxytoca*, C) *Pseudomonas aeruginosa*, D) *Staphylococcus aureus*, E) *Streptococcus mutans* and F) *Bacillus subtilis*.

52.99% at the highest concentration of AgNPs (5 mM). AgNPs were more bactericidal in liquid than the solid medium, due a better contact with bacterial cells. Figure 9 shows the percentage of dust inhibition by the turbidimetry method, in this graph it can be observed that the higher the concentration of AgNPs there is a higher percentage of inhibition.

Regarding the number of bacterial colonies inhibited by composites at different concentrations of AgNP in Figure 9, they show that the minimum inhibitory concentration (MIC) for *E. coli*, *K. oxytoca*, *P. aeruginosa*, *S. Mutans*, *S. aureus*, and *B. Subtilis* is 0.5 mM. As seen in Figure 9, the growth of *E. coli* was inhibited from 24.08 to 41.50%, *K. oxytoca* was inhibited

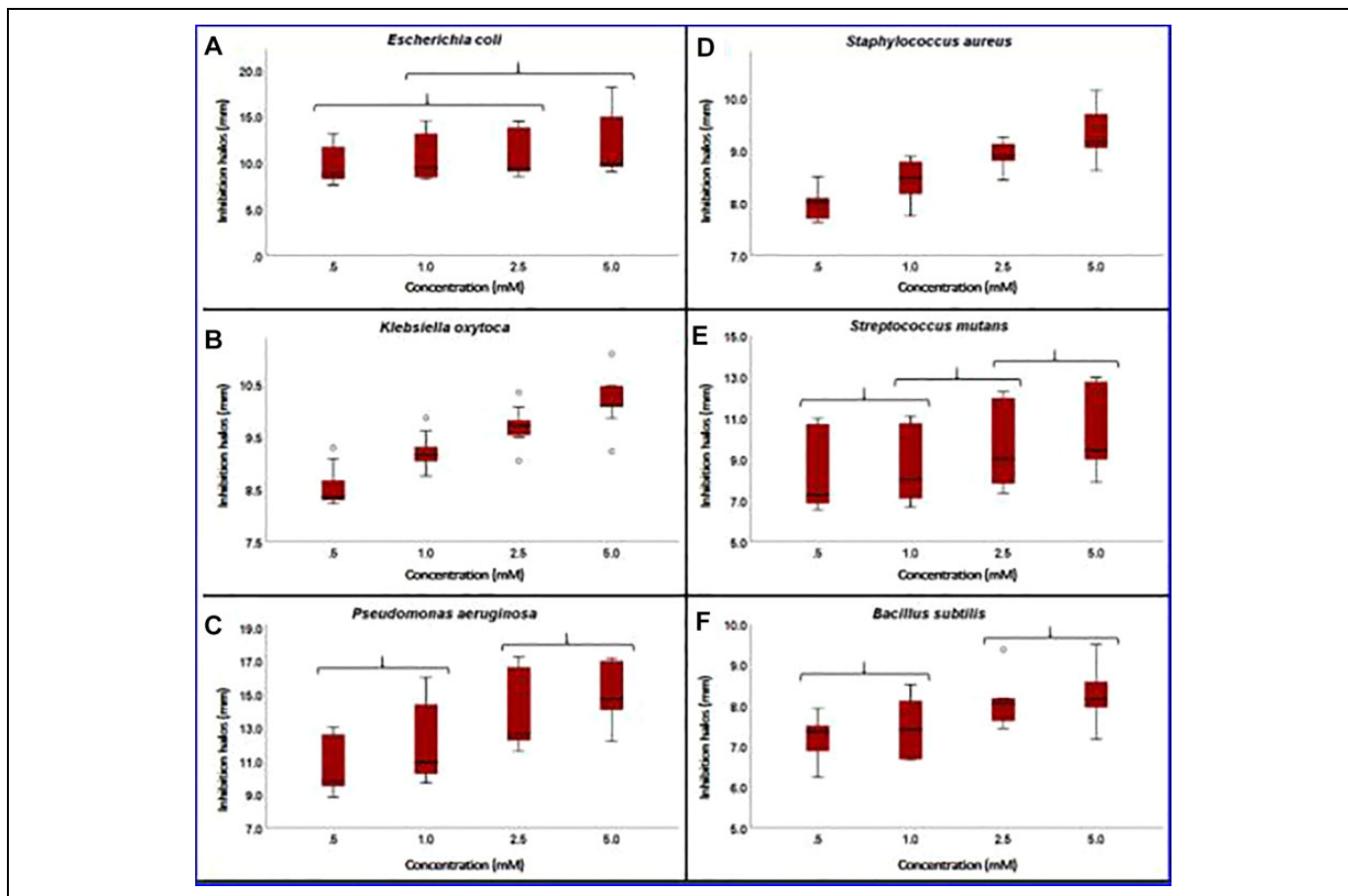


Figure 8. Box Plot of the inhibition halo of HAp-AgNPs powders.

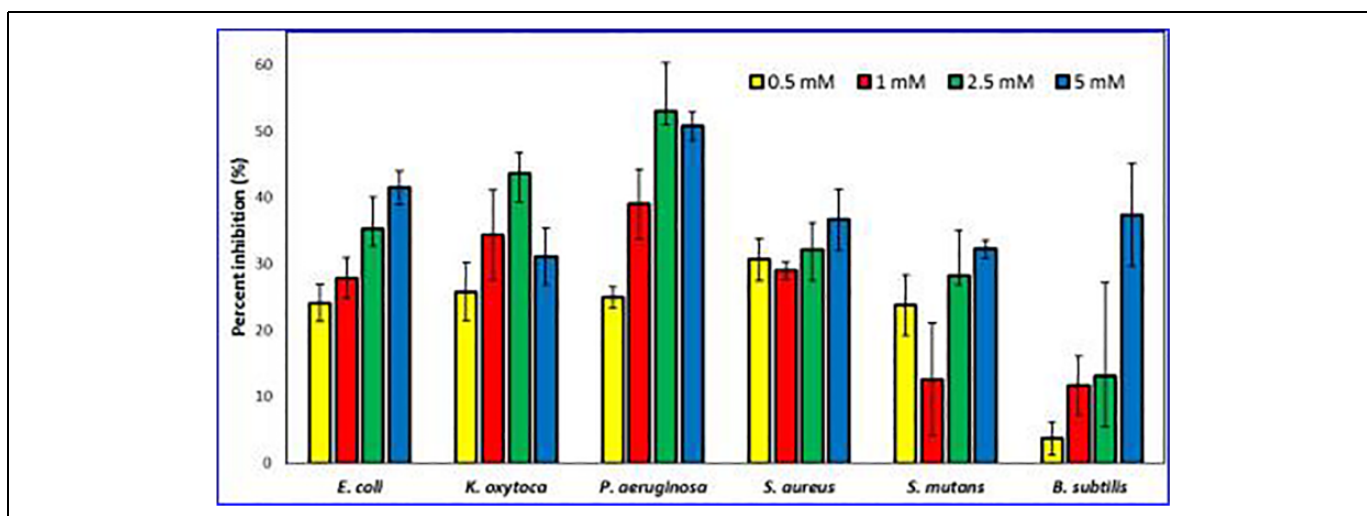


Figure 9. Percent inhibition of HAp-AgNPs powders.

by 25.77 to 43.59%, the growth inhibited for *P. aeruginosa* was from 25.02 to 50.74%; in *S. aureus* it was around 28.97 to 36.66%, inhibition of growth of was 12.60 to 32.22% for *S. Mutans* and finally in *B. Subtilis* was around 3.73 to 37.39% for concentrations from 0.5 to 5 mM respectively.

Through a Tukey analysis (see Figure 10) with a significance level of 0.05 and using the absorbance obtained as a response variable, it was observed that from the concentration of 0.5 mM a significant effect was obtained in the inhibition for *E. coli*, *S. aureus* and *P. aeruginosa*, while for *K. oxytoca* there

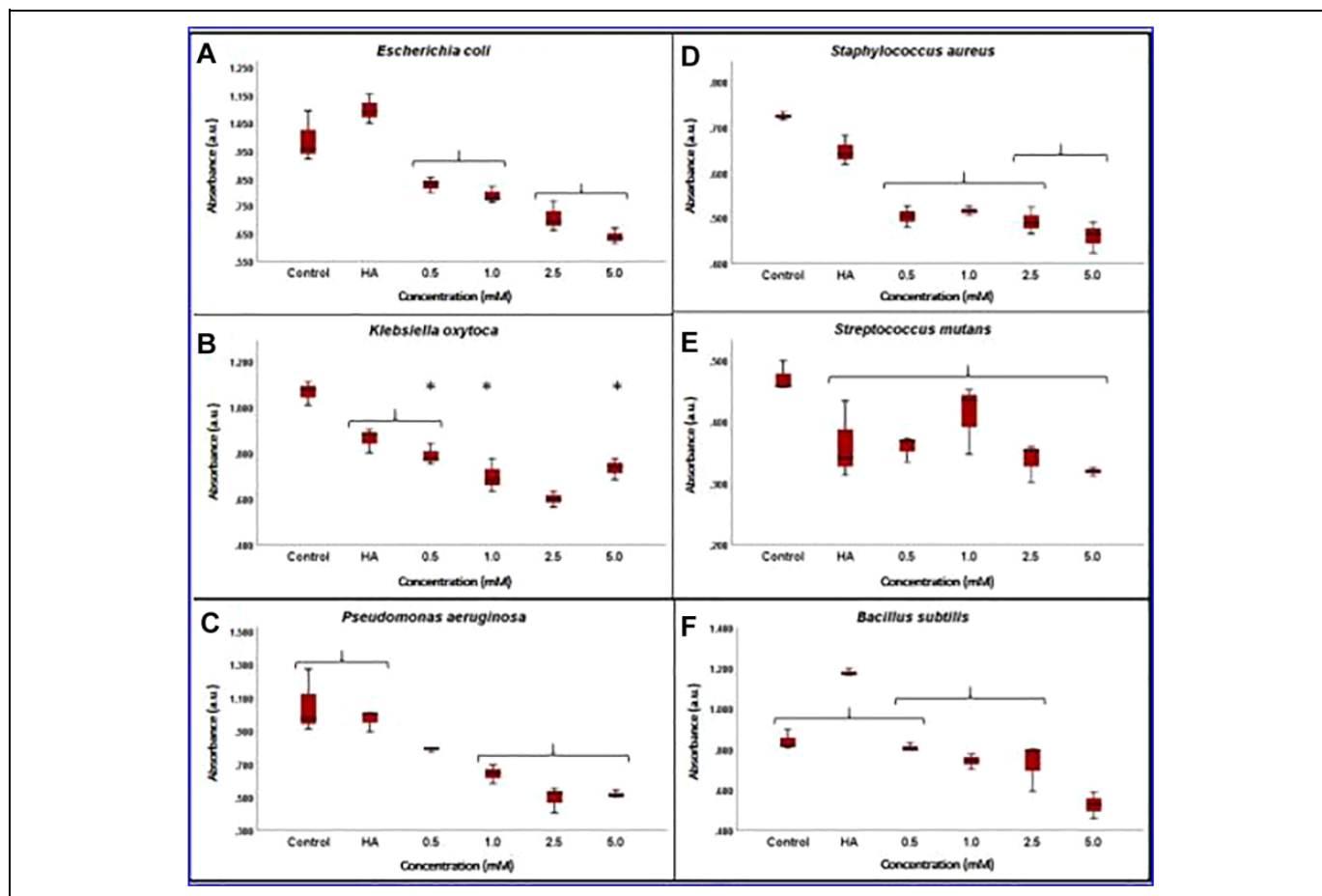


Figure 10. Box Plot of the inhibition of HAp-AgNPs powders.

is no significant difference between the lowest concentration and the HA, *S. mutans* has no significant difference between the concentrations and the HA, *B. subtilis* don't has a significant difference between the lowest concentration and the control. For *E. coli*, *S. aureus* and *B. subtilis* a growth is observed with the presence of HAp. In studies, a very strong bactericidal effect of silver nanoparticles has been seen, against *Escherichia coli*, *Enterococcus*, *Staphylococcus aureus* and *Candida albicans* showing the great effectiveness of silver on a nanometric scale.^{7,8} The effectiveness of composites obtained is demonstrated, the composites showed better activity against Gram-negative than Gram-positive bacteria that is due to the thickness of the peptidoglycan layer, which may prevent the action of silver through the bacterial cell wall in accordance with the results reported in other investigations.

The suggested mechanism of action of nanoparticles on bacteria is the production of changes in the morphology of the cell membrane. Studies have shown that nanoparticles penetrate bacteria and that their diffusion is directly proportional to the size and morphology of the nanoparticles. A smaller Nps, greater the damage and the possibility of permeating, damaging the membrane. The existence of ion channels and transporter proteins have been reported to aid the passage of nanoparticles through the plasma membrane. The antibacterial effects of

nanoparticles reported are: 1) alteration of the bacterial cell membrane; 2) generation of ROS; 3) penetration of the bacterial cell membrane; and 4) induction of intracellular antibacterial effects, including interactions with DNA and proteins.¹⁸

Antibacterial activities gradually increase with increasing Ag content. Ag nanoparticles start and increased the development of reactive oxygen species (ROS) leading to the destruction of bacteria. High levels of ROS have many special effects on bacteria, such as lipid peroxidation affecting the integrity of the bacterial membrane, resulting in a high level of ion permeability. The positive ions released from the nanoparticles disrupt the stability of the cell which eventually leads to death.^{4,8,11,18,20,21} Antibacterial properties indicated that HAp-AgNPs do not exhibit the same antibacterial effect in Gram positive bacteria in contrast to Gram negative bacteria. The bactericidal efficacy of AgNPs also depends on the bacterial strains. AgNPs have greater antibacterial activity against Gram negative bacteria than Gram positive bacteria due to the difference in the structures of their cell walls. The cell wall of Gram negative bacteria is quite thin (<10 nm), consisting of a single layer of peptidoglycan, which makes infiltration of Ag⁺ ions into the membrane easy. In contrast, Gram positive bacteria possess a thicker peptidoglycan layer (20–80 nm) than Gram negative bacteria, acting as a barrier to the penetration

Table 1. Literature Review of Research on the Bactericidal Effect of Silver and Silver Nps.

Referencia	Material	Inoculum	Particle size (nm)	Concentration AgNPs	Bacterium/(MIC)
Present work	HA-AgNPs	1.3×10^6 CFU/mL	5.6 ± 2.9	0.5 mM (0.027 mg/g), 1.0 mM (0.054 mg/g), 2.5 mM (0.135 mg/g) 5.0 mM (0.270 mg/g)	<i>E. coli</i> / >0.5 mM <i>S. mutans</i> / > 0.5 mM <i>E. aureus</i> / > 0.5 mM <i>K. oxytoca.</i> / > 0.5 nM <i>P. aeruginosa</i> / > 0.5 mM <i>B. subtilis</i> / > 0.5 mM <i>E. coli</i> / >3.3 nM <i>S. aureus</i> / >33 nM
Kim et al. <i>Nanomedicine</i> , 2007; 3(1):95–101. ²⁸	Silver nanoparticles	10^7 CFU/ mL	13.4 ± 2.6	0.2 – 33 nM	<i>E. coli</i> / >3.3 nM <i>S. aureus</i> / >33 nM
Raffi et al., <i>J Mater Sci Technol</i> . 2008; 24 (2):192–196. ²⁹	Silver nanoparticles	10^4 CFU/mL	16	0, 20, 40, 60, 80 and 100 μ g/mL	<i>E. coli</i> / 20 μ g/ml Inhibit colony-forming unit at 60 μ g/mL
Nirmala, R., et al., <i>Journal of Nanoparticle Research</i> , (2010) 13(5), 1917–1927. ³⁰	Bovine femur bone hydroxyapatite-silver nanoparticles	$1.5 \times 10^{6-8}$ UFC/mL	8–20	0, 1, 3, and 5%	<i>E. coli</i> / 3% MRSA / 1%
Mocanu, A, et al., <i>Applied Surface Science</i> , (2014) 298, 225–235. ³¹	Nano hydroxyapatite doped with silver	10^6 UFC/ml	12.0 ± 5.0	2, 2.5, 3, 3.6, 4.5 and 5.4%	<i>E. coli</i> / 2% of 10 mm of inhibition <i>S. aureus</i> / 2% 11 mm of inhibition
Pazos-Ortiz, E., et al., <i>Journal of Nanomaterials</i> , Volume 2017, 7 pages, ID 485121. ²²	PCL-AgNPs	1.3×10^6 CFU/mL	5.6 ± 2.9	12.5 mM (0.012 mg/g), 25.0 mM (0.024 mg/g), 50.0 mM (0.046 mg/g) 100.0 mM (0.097 mg/g)	<i>E. coli</i> / > 12.5 mM <i>E. aureus</i> / > 12.5 mM <i>K. oxytoca.</i> / > 12.5 mM <i>P. aeruginosa</i> / > 12.5 mM
Riaz et al., <i>Materials Science and Engineering: C</i> , (2018) 90, 308-313. ³²	Silver doped hydroxyapatite	10^5 CFU/mL	-	0, 0.1, 0.3, 0.5, 0.7 M of AgNO_3	<i>S. aureus</i> / 0.1 M
Biao, L. et al., <i>Colloids and Surfaces B: Biointerfaces</i> , (2018) 169, 438-443. ³³	Proanthocyanidins- functionalized Ag nanoparticles	10^8 CFU/mL	33.2 ± 5.6	0.49 to 62.8 μ g/mL	<i>E. coli</i> / 3.92 μ g/ml <i>S. aureus</i> / 1.96 μ g/ml
Zhou, Q. et al. <i>Colloids and Surfaces A: Physicochemical and Engineering Aspects</i> , (2020) 585, 124081. ³⁴	HApNPs	10^5 CFU/mL	-	0.01 M, 0.05 M, and 0.1 M of AgNO_3	<i>E. coli</i> / 0.01 M <i>S. aureus</i> / 0.01 M
Menazea, A. A., et al., <i>Applied Surface Science</i> , (2020) 145299. ³⁵	AgNPs@Se-CHAP/PCL composite fibers	1.5×10^8 CFU/mL	80 - 140	Depositions at time of 5, 10, 15, and 20 min.	<i>E. coli</i> / 40% of inhibition at 10 min <i>S. aureus</i> / 42% of inhibition at 15 min

of Ag^+ ions into the cytoplasm.^{4,8,20,21} An Additional distinction of Gram-positive bacteria is that they contain teichoic acid bound to the cell wall by a covalent bond.

Uncontrolled bacterial growth is due to the increased prevalence of biofilms that help microorganisms to survive in hostile environments. In this way, biofilms confer resistance to antimicrobial agents and the immune system, causing persistent and chronic infections. Biofilms are also a major cause of medical infections associated with implants. The microorganisms are developing resistance to the drug, new developments in composites given the opportunity to be an alternative to contrast the diseases caused by resistant microorganisms. Silver NPs have greater advantages as antibacterial agents because their surface area is extremely large, and they can easily penetrate biofilms. Bacterial cell membranes are destroyed by the presence of

metallic nanomaterials. The normal structure of proteins or enzymes in the membrane are similar to the cell wall, the enzymes contain sulfur in thiol groups (-SH) that react with silver atoms producing stable S-Ag bonds, causing inactivation of the cell membrane and of the proteins responsible for transmembrane energy generation and ion transport.⁸ The nanoparticles produce the inhibition of exopolysaccharides and capsule-forming proteins, which causes greater bacterial death. Also, the interaction of nanoparticles or their metal ions with the bacterial cell walls surface causing death on contact, the mechanism that occurs due to the negative charge on the cell wall of bacteria, and probably this the most important antibacterial mechanism caused by electrostatic interaction.

Silver is known to have antibacterial activity throughout history, against gonococcal infections. Silver cation has been

reported to have a much greater antibacterial effect than AgNps. Table 1 shows a literature review of research on the bactericidal effect of silver, where the contribution and competitiveness of powders obtained is observed against the bacteria tested at low concentration. However, Ag cations have limited utility as an antimicrobial agent due to the formation of precipitates due to the low solubility of their salts, which is why a continuous antimicrobial mechanism would be achieved if you have a controlled release of Ag ions. In this research low concentrations are used to demonstrate the competitiveness of synthesis developed, for example, the concentration of 5 mM has an equivalent of 0.027 mg Ag/g and the composite allows the controlled release of silver of 0.065 mg/ml for turbidimetry method. Silver is becoming a therapeutic arsenal against the emergence of antibiotic-resistant bacteria and its increasing prevalence in hospitals. The use of silver has been severely limited by the toxicity of silver ions; however, nanotechnology offers an advantage of using low metal concentrations with greater bactericidal action. The composites of HAp-AgNPs can be used to treat or prevent infections or orthopedic devices counteracting resistant bacterial infections by the formation of biofilms.

Conclusion

The synthesis of nanocomposites provides an innovative, latent, and efficient platform to address antibiotic resistance transforming the field of Nanomedicine, with potential to attack infections resistant to multiple drugs. Chemical synthesis proposed for silver nanoparticles from non-toxic carboxylic acids such as gallic acid provides easy, environmentally friendly and easy scaled method, because this synthesis route does not need to use drastic reaction conditions such as: high pressure, energy consumption, temperature and toxic reagents. In this way, the synthesis of HAp and AgNPs using the presented methodology is an easy way and with less environmental damage. HAp and HAp-Ag composites have been successfully prepared by the sol-gel and chemical green method. The reduction of aqueous Ag^+ ions by gallic acid and results of UV-visible spectroscopy, DLS and STEM showed the presence of silver nanoparticles of well-defined dimensions with diameters around 6 nm. X-ray diffraction analysis shows the formation of crystalline HA. Energy dispersive X-ray spectroscopy and SEM confirmed the presence of distributed silver agglomerates on the surface of the hydroxyapatite powders. All HAp-AgNPs powders showed a good and specific antibacterial effect despite the low concentration of silver used. HAp-AgNPs compounds may have a high potential for medical treatments centered on the control of diseases of bacteria that have presented resistance to antibiotics.

Acknowledgments:

Thanks to PRODEP, Universidad Autónoma de Ciudad Juárez and CONACYT.

Declaration of Conflicting Interests

The author(s) declared no potential conflicts of interest with respect to the research, authorship, and/or publication of this article.

Funding

The author(s) received no financial support for the research, authorship, and/or publication of this article.

ORCID iD

Simón Yobanny Reyes-López  <https://orcid.org/0000-0002-9017-3233>

References

1. López-Esparza J, Espinosa-Cristóbal LF, Donohue-Cornejo A, Reyes-López SY. Antimicrobial activity of silver nanoparticles in polycaprolactone nanofibers against gram-positive and gram-negative bacteria. *Ind Eng Chem Res*. 2016;55(49):12532-12538. doi:10.1021/acs.iecr.6b02300
2. Yun JE, Lee DG. *Silver Nanoparticles: A Novel Antimicrobial Agent. Antimicrobial Nanoarchitectonics: From Synthesis to Applications*. Elsevier Inc. 2017:139-166. doi:10.1016/B978-0-323-52733-0.00006-9
3. Khan SU, Saleh TA, Wahab A, et al. Nanosilver: new ageless and versatile biomedical therapeutic scaffold. *Int J Nanomedicine*. 2018;13:733-762.
4. Muñoz-Escobar A, Ruíz-Baltazar AD, Reyes-López SY. Novel route of synthesis of PCL-CuONPs composites with antimicrobial properties. *Dose Response*. 2019;17(3). doi:10.1177/1559325819869502
5. Yuan Q, Xu A, Zhang Z, et al. Bioactive silver doped hydroxyapatite composite coatings on metal substrates: synthesis and characterization. *Mater Chem Phys*. 2018;218:130-139. doi:10.1016/j.matchemphys.2018.07.038
6. Tian B, Chen W, Dong Y, et al. Silver nanoparticle-loaded hydroxyapatite coating: structure, antibacterial properties, and capacity for osteogenic induction in vitro. *RSC Adv*. 2016;6(11):8549-8562.
7. Zhang XF, Liu ZG, Shen W, Gurunathan S. Silver nanoparticles: synthesis, characterization, properties, applications, and therapeutic approaches. *Int J Mol Sci*. 2016;17(9):1534.
8. Makvandi P, Wang C, Zare EN, Borzacchiello A, Niu L, Tay FR. Metal-Based nanomaterials in biomedical applications: antimicrobial activity and cytotoxicity aspects. *Adv Funct Mater*. 2020:1910021.
9. Burduşel AC, Gherasim O, Grumezescu AM, Mogoantă L, Ficai A, Andronesu E. Biomedical applications of silver nanoparticles: an up-to-date overview. *Nanomaterials*. 2018;8(9):681.
10. Qasim M, Udomluck N, Chang J, Park H, Kim K. Antimicrobial activity of silver nanoparticles encapsulated in poly-N-isopropylacrylamide-based polymeric nanoparticles. *Int J Nanomedicine*. 2018;13:235-249.
11. Liu X, Mou Y, Wu S, Man HC. Synthesis of silver-incorporated hydroxyapatite nanocomposites for antimicrobial implant coatings. *Appl Surf Sci*. 2013;273:748-757. doi:10.1016/j.apsusc.2013.02.130

12. Roque-Ruiz JH, Castillo-Ramírez D, Ruíz-Baltazar ÁDJ, Espinosa-Cristóbal LF, eyes-López SY. Preparation of silver-doped alumina spherical beads with antimicrobial properties. *J Nanometer*. 2018;2018.
13. Kim H, Mondal S, Jang B, Manivasagan P, Moorthy MS, Oh J. Biomimetic synthesis of metal-hydroxyapatite (Au-HAp, Ag-HAp, Au-Ag-HAp): structural analysis, spectroscopic characterization and biomedical application. *Ceram Int*. 2018;44(16):20490-20500. doi:10.1016/j.ceramint.2018.08.045
14. Ruíz-Baltazar ÁDJ, Reyes-López SY, Silva-Holguín PN, Larrañaga D, Estévez M, Pérez R. Novel biosynthesis of Ag-hydroxyapatite: structural and spectroscopic characterization. *Results Phys*. 2018;9:593-597. doi:10.1016/j.rinp.2018.03.016
15. Riaz M, Zia R, Ijaz A, Hussain T, Mohsin M, Malik A. Synthesis of monophasic Ag doped hydroxyapatite and evaluation of antibacterial activity. *Mater Sci Eng C*. 2018;90:308-313. doi:10.1016/j.msec.2018.04.076
16. Thamaraiselvi T, Rajeswari S. Biological evaluation of bioceramic materials—a review. *Trends Biomater Artif Organs*. 2004;18(1):9-17.
17. Park J, Cha SH, Cho S, Park Y. Green synthesis of gold and silver nanoparticles using gallic acid: catalytic activity and conversion yield toward the 4-nitrophenol reduction reaction. *J Nanopart Res*. 2016;18(6):166.
18. Wang L, Hu C, Shao L. The antimicrobial activity of nanoparticles: present situation and prospects for the future. *Int J Nanomedicine*. 2017;12:1227-1249.
19. Ruíz-Baltazar Á, Reyes-López SY, Larrañaga D, Estévez M, Pérez R. Green synthesis of silver nanoparticles using a *Melissa officinalis* leaf extract with antibacterial properties. *Results Phys*. 2017;7:2639-2643.
20. Precious Ayanwale A, Reyes-López SY. ZrO₂-ZnO nanoparticles as antibacterial agents. *ACS Omega*. 2019;4(21):19216-19224. doi:10.1021/acsomega.9b02527
21. Garibay-Alvarado JA, Espinosa-Cristóbal LF, Reyes-López SY, Fibrous Silica-Hydroxyapatite Composite by Electrospinning. *Int J Res - GRANTHAALAYAH*, 2017;5(2):39-47.
22. Pazos-Ortiz E, Roque-Ruiz JH, Hinojos-Márquez EA, López-Esparza J, Donohué-Cornejo A, Cuevas-González JC, Espinosa-Cristóbal LF, Reyes-López SY. Dose-dependent antimicrobial activity of silver nanoparticles on polycaprolactone fibers against gram-positive and gram-negative bacteria. *J Nanomater*. 2017;2017(6): 7.
23. Jayaramudu T, Raghavendra GM, Varaprasad K, Sadiku R, Ramam K, Raju KM. Iota-Carrageenan-based biodegradable Ag₀ nanocomposite hydrogels for the inactivation of bacteria. *Carbohydr Polym*. 2013;95(1):188-194. doi:10.1016/j.carbpol.2013.02.075
24. Loher S, Schneider OD, Maienfisch T, Bokorny S, Stark WJ. Micro-organism-triggered release of silver nanoparticles from biodegradable oxide carriers allows preparation of self-sterilizing polymer surfaces. *Small*. 2008;4(6):824-832. doi:10.1002/smll.200800047
25. Richter AP, Brown JS, Bharti B, et al. An environmentally benign antimicrobial nanoparticle based on a silver-infused lignin core. *Nat Nanotechnol*. 2015;10(9):817-823. doi:10.1038/nnano.2015.141
26. Sarwar MS, Niazi MBK, Jahan Z, Ahmad T, Hussain A. Preparation and characterization of PVA/nanocellulose/Ag nanocomposite films for antimicrobial food packaging. *Carbohydr Polym*. 2018;184:453-464. doi:10.1016/j.carbpol.2017.12.068
27. Kim JS, Kuk E, Yu KN, et al. Antimicrobial effects of silver nanoparticles. *Nanomedicine*. 2007;3(1):95-101.
28. Raffi M, Hussain F, Bhatti T, Akhter J, Hameed A, Hasan M. Antibacterial characterization of silver nanoparticles against *E. coli* ATCC-15224. *J Mater Sci Technol*. 2008;24(2):192-196.
29. Nirmala R, Sheikh FA, Kanjwal MA, et al. Synthesis and characterization of bovine femur bone hydroxyapatite containing silver nanoparticles for the biomedical applications. *J Nanopart Res*. 2010;13(5):1917-1927.
30. Mocanu A, Furtos G, Rapuntean S, et al. Synthesis; characterization and antimicrobial effects of composites based on multi-substituted hydroxyapatite and silver nanoparticles. *Appl Surf Sci*. 2014;298:225-235.
31. Riaz M, Zia R, Ijaz A, Hussain T, Mohsin M, Malik A. Synthesis of monophasic Ag doped hydroxyapatite and evaluation of antibacterial activity. *Mater Sci Eng C*. 2018;90:308-313.
32. Biao L, Tan S, Zhang X, Gao J, Liu Z, Fu Y. Synthesis and characterization of proanthocyanidins-functionalized Ag nanoparticles. *Colloids Surf B: Biointerfaces*. 2018;169:438-443.
33. Zhou Q, Wang T, Wang C, et al. Synthesis and characterization of silver nanoparticles-doped hydroxyapatite/alginate microparticles with promising cytocompatibility and antibacterial properties. *Colloid Surfaces A Physicochemical Eng Aspects*. 2020;585:124081.
34. Menazea AA, Abdelbadie SA, Ahmed MK. Manipulation of AgNPs coated on selenium/carbonated hydroxyapatite/ε-poly-caprolactone nano-fibrous via pulsed laser deposition for wound healing applications. *Appl Surf Sci*. 2020;508:145299.
35. Qing Y, Cheng L, Li R, et al. Potential antibacterial mechanism of silver nanoparticles and the optimization of orthopedic implants by advanced modification technologies. *Int J Nanomedicine*. 2018;13:3311-3327.